RESEARCH ARTICLE

Ether chain functionalized fullerene derivatives as cathode interface materials for efficient organic solar cells

Jikang LIU, Junli LI, Guoli TU (✉)

Wuhan National Laboratory for Optoelectronics, Huazhong University of Science and Technology, Wuhan 430074, China

Abstract The electron transport layer (ETL) plays a crucial role on the electron injection and extraction, resulting in balanced charge transporting and reducing the interfacial energy barrier. The interface compatibility and electrical contact via employing appropriate buffer layer at the surface of hydrophobic organic active layer and hydrophilic inorganic electrode are also essential for charge collections. Herein, an ether chain functionalized fullerene derivatives [6,6]-phenyl-C_{61}-butyricacid-(3,5-bis(2-(2-ethoxyethoxy)-ethoxy)-phenyl)-methyl ester (C_{60}-2EPM) was developed to modify zinc oxide (ZnO) in inverted structure organic solar cells (OSCs). The composited ZnO/C_{60}-2EPM interface layer can help to overcome the low interface compatibility between ZnO and organic active layer. By introducing the C_{60}-2EPM layer, the composited fullerene derivatives tune energy alignment and accelerated the electronic transfer, leading to increased photocurrent and power conversion efficiency (PCE) in the inverted OSCs. The PCE based on PTB7-Th:$PC_{71}BM$ was enhance from 8.11% on bare ZnO to 8.38% and 8.65% with increasing concentrations of 2.0 and 4.0 mg/mL, respectively. The fullerene derivatives C_{60}-2EPM was also used as a third compound in P3HT:$PC_{61}BM$ blend to form ternary system, the devices with addition of C_{60}-2EPM exhibited better values than the control device.

Keywords interface compatibility, functionalized fullerene derivatives, tune energy alignment, third compound, ternary system

1 Introduction

Bulk-heterojunction (BHJ) organic solar cells (OSCs) have exhibited significant advantages of lightweight, low cost and high mechanical flexibility for large-scale commercia-

lization [1–7]. For the BHJ OSCs devices, the active layer is fabricated in a way toward maximized interfacial contact areas by controlling the ratio of electron-donating polymer and electron-accepting molecule, usually a fullerene derivative [8–12].

Zinc oxide (ZnO) has been widely used as an interface buffer layer material to modify the cathode electrode in inverted architecture OSCs devices. Relying on its low work function, ZnO could form an ohmic contact with the active layer by introducing in OSCs devices [13–15]. However, ZnO was also found to be strongly dependent on its surface properties, such as the trap and defects [16–18]. To get higher power conversion efficiency (PCE) of OSCs, the modification of ZnO has been an important strategy for the optimization in inverted OSCs [19–21]. An effective way to overcome this problem is introducing a modifying layer of organic molecules on ZnO, such as fullerene derivatives [22–24]. Fullerene derivatives with functional groups, such as ammonium salt, ether, ester groups and carboxylic acid, have been widely used to modify the ZnO layer [25–30]. The fullerene derivatives can be processed through a solution-based spin-coating method, which demonstrated good compatibility between organic active layer and metal oxide [31]. It is believed that the incorporation of fullerene derivative layer between the ZnO and active layer can be benefit for the collection of electron and enhancement of device performance [32–34]. The fullerene derivatives which have a good solution in chlorobenzene can be also used as an additive to form ternary system in OSCs [35].

Herein, we designed and synthesized an ether chain functionalized fullerene derivatives [6,6]-phenyl-C_{61}-butyricacid-(3,5-bis(2-(2-ethoxyethoxy)ethoxy)phenyl) methyl ester (C_{60}-2EPM) and applied as a modification layer on ZnO cathode buffer layer (CBL) in inverted OSCs devices. The inverted devices composed of poly[4,8-bis(5-(2-ethylhexyl)thiophen-2-yl)benzo[1,2-b;4,5-b']dithiophene-2,6-diyl-alt-(4-(2-ethylhexyl)-3-fluorothieno [3,4-b] thiophene-)-2-carboxylate-2-6-diyl)] (PTB7-Th):[6,6]-phenyl-C_{71}-butyric acid methyl ester ($PC_{71}BM$) showed

better device performance by using the ZnO/ fullerene derivatives electron transport layer formed by one-step spin-coating technique than control device. When fullerene derivatives with ions groups (such as sulfonate, ammonium, phosphate) spin-coated on ZnO, the ions may incorporate in photovoltaic layer and decrease the lifetime of primary exciton, which can be explained by the formation of charge-transfer states that stabilized by the coulomb field of ions [36]. However, the application of ether chain functionalized fullerene derivatives C_{60}-2EPM may avoid the phenomenon of ions migration, and guarantee the lifetime and stability of device. The fullerene derivatives C_{60}-2EPM have selected solubility and can support mutil-layer OSCs structures by solutions processing. The existence of large amount of fullerene derivatives in cathode interface layer were expected to form a multi transporting channels for electrons and decrease the hole quenching at the cathode for the polymer: fullerene solar cells (Fig. 1). With two concentrations (2.0 and 4.0 mg/mL) of C_{60}-2EPM applied in inverted OSCs with structure of ITO/ZnO/fullerene derivative/PTB7-Th:PC_{71}BM/MoO_3/Al, it was found that the PCE of the devices could be obvious enhanced to 8.38% and 8.65% compared with 8.11% of bare ZnO. The C_{60}-2EPM was also used as an additive in poly (3-hexylthiophene) (P3HT):phenyl-C_{61}-buty-ric acid methyl ester (PC_{61}BM) system to form a ternary system, the devices with 5%, 10%, 15% and 20% additions of C_{60}-2EPM have got PCEs of 3.64%, 3.84%, 3.87% and 3.76% compared with the control device (PCE of 3.49%).

2 Experimental

2.1 Materials

[6,6]-Phenyl-C_{61}-butyricacidmethylester (PC_{61}BM) was purchased from Luminescence Technology Corp. 1,2-Dichlorobenzene (ODCB) was purchased from Aladdin Industrial Corp (99.0% purity). Other reagents and solvents were purchased from Sinopharm Chemical Reagent and used without further purification unless noted.

2.2 Synthesis

The synthetic route of fullerene derivative C_{60}-2EPM was outlined in Scheme 1.

2.2.1 Synthesis of PC_{61}BA

The synthesis was synthesized according to Refs. [37–39].

2.2.2 Synthesis of 2EPM

The reactants of 5-(hydroxymethyl) benzene-1,3-diol (3.36 g, 24 mmol), 2-(2-ethoxyethoxy)-ethyl bromide (14.18 g, 72 mmol), potassium acetate (9.96 g, 72 mmol), and 18-crown-6 (0.1 g, 0.37 mmol) were dissolved in dry acetone (100 mL) under nitrogen. With stirring at 100°C for 48 h, the mixture solution was extracted with dichloromethane (DCM) and washed with brine, then dried with anhydrous magnesium sulfate for three times in a separating funnel. The crude product was purified by silica gel column chromatography with a mixture of petroleum ether (PE) : ethyl acetate (EA) = 4:1 as eluent to obtain the pure product 7.13 g (yield, 80%). ^{1}H NMR (600 MHz, CDCl3) : 1.22 (5.8H, t, J = 7.02 Hz), 3.54 (3.8H, q, J = 7.00 Hz), 3.62 (3.1H, d, J = 3.36 Hz), 3.71 (3.3H, d, J = 5.04 Hz), 3.72 (3.7H, d, J = 6.12 Hz), 3.85 (3.4H, d, J = 4.92 Hz), 4.12 (3.8H, d, J = 9.72 Hz), 6.42 (0.9H, d, J = 2.04 Hz), 6.54 (1.8H, d, J = 1.98 Hz).
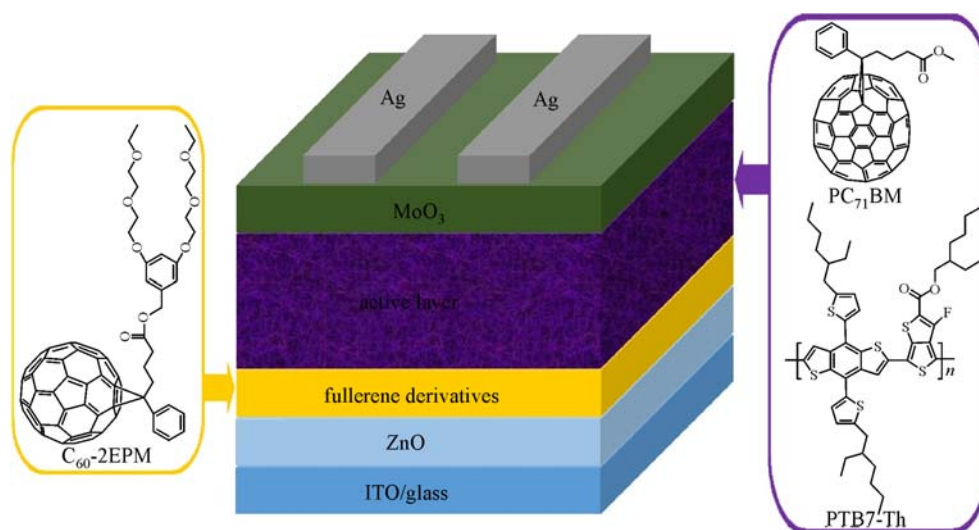

Fig. 1 Device architecture of the inverted organic solar cells and molecular structures of C_{60}-2EPM, PC_{71}BM and PTB7-Th

2.2.3   Synthesis of C$_{60}$-2EPM

PC$_{61}$BA (100 mg, 0.112 mmol) and 2EPM (83 mg, 0.224 mmol) were dissolved in dry O-dichlorobenzene (ODCB) (15 mL). The solution was sonicated for 5 min to dissolve PC$_{61}$BA completely. Then N,N'-dicyclohexylcarbodiimide (DCC) (21 mg, 0.102 mmol) and the 4-dimethylaminopyridine (DMAP) (12 mg, 0.098 mmol) were added to the solution. The obtained solution was allowed to stir at 0°C for 24 h and stir at room temperature for another 24 h. The solvent was removed in vacuo and the crude product was purified by silica gel column chromatography with a mixture of petroleum ether (PE) : ethyl acetate (EA) = 2:1 as eluent to obtain the pure product 98 g (yield, 70%). ^{1}H NMR (600 MHz, CDCl3) : 1.21 (5.6H, t, J = 6.99 Hz), 2.20 (1.1H, d, J = 7.92 Hz), 2.21 (0.9H, d, J = 4.50 Hz), 2.58 (1.7H, t, J = 7.41 Hz), 2.91 (1.0H, d, J = 5.04 Hz), 2.92 (1.2H, d, J = 7.98 Hz), 3.53 (3.5H, q, J = 7.00 Hz), 3.62 (3.2H, d, J = 5.04 Hz), 3.71 (3.5H, d, J = 9.48 Hz), 3.84 (3.0H, d, J = 4.80 Hz), 4.10 (3.3H, d, J = 9.54 Hz), 6.49 (1.5H, d, J = 1.32 Hz), 7.48 (0.8H, d, J = 7.38 Hz), 7.54 (1.8H, t, J = 7.56 Hz), 7.92 (1.6H, d, J = 7.56 Hz).

2.3   Chemical properties

2.3.1   Characterization of ^{1}H NMR spectrums

The ^{1}H NMR spectrums of 2EPM and C$_{60}$-2EPM were showed in Figs. S1 and S2, the solvent was dichloroformate. For 2EPM, the δ = 3.51 – 4.10 ppm[1] was corresponding to chemical shift of the ten CH$_2$ on ether chain, and δ = 1.20 – 1.22 ppm was corresponding to chemical shift of the two methyl (CH$_3$) on ether chain. For C$_{60}$-2EPM, the δ = 2.90 – 2.93 ppm, 2.56 – 2.59 ppm and 2.19 – 2.21 ppm were corresponding to chemical shift of the three methylene (CH$_2$) on PC$_{61}$BA. The δ = 3.51 – 4.10 and δ = 1.20 – 1.22 ppm were same with ^{1}H NMR spectrums of 2EPM. Compared with the ^{1}H NMR spectrums of 2EPM and C$_{60}$-2EPM, it concluded that the fullerene derivatives of C$_{60}$-2EPM have been obtained successfully.

2.3.2   Characterization of UV-visible absorption

To confirm the structure of C$_{60}$-2EPM further, the measurement of UV-visible absorption of the PC$_{61}$BA, 2EPM and C$_{60}$-2EPM were taken. In Fig. S3, a sharp absorption caused by the benzene structure appeared at 269 nm in the absorption of 2EPM. There were two peaks from the absorption of PC$_{61}$BA (330 and 435 nm), which were identified as the characteristic absorption peak of PC$_{61}$BA. From the absorption of C$_{60}$-2EPM, it was found that the absorption peaks were almost similar with PC$_{61}$BA. The author supported that the chemical properties of C$_{60}$-2EPM were mainly determined by PC$_{61}$BA. Compared with the characteristic absorption peak in UV-
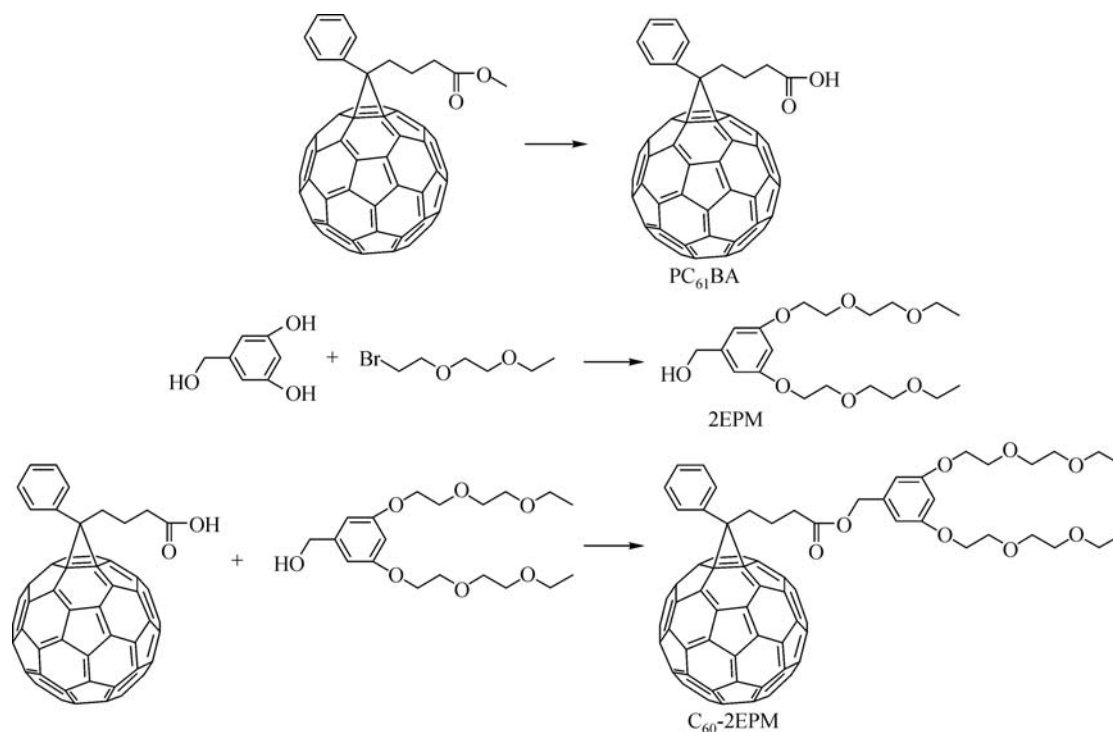
Scheme 1   Synthetic scheme of C$_{60}$-2EPM

---

1) 1 ppm = 10^{-6}

visible absorption spectra of $PC_{61}BA$ and 2EPM, the absorption spectra of the C_{60}-2EPM were also evidence to confirm the structure of C_{60}-2EPM.

2.4   Device fabrication

Indium tin oxide (ITO) conductive glass (19 Ω/cm^2) was cleaned by sequentially ultrasonication in detergent, deionized water, acetone and isopropyl, then blew by nitrogen and dried in oven at 80°C overnight. The substrates then underwent 10 min UV–O_3 treatment and were transferred into a glove box with N_2 atmosphere. Then ZnO films on ITO were fabricated as follows: The ZnO precursor solutions were prepared by dissolving zinc acetate dehydrate (0.98 g) in a mixture of 2-methoxyethanol (10 mL) as the solvent and ethanolamine (275 μL) as the stabilizer under sufficient stirring overnight. The transparent precursor solution then was spin-coated onto the ITO substrates at 3500 r/min for 35 s, followed by annealing at 220°C for 30 min in air to give a thin film of ZnO. Then the substrates were transferred into a glovebox and naturally cooled to room temperature.

2.4.1   Fabrication of inverted OSCs with fullerene derivatives as ETL

The fullerene derivatives C_{60}-2EPM with the connection of 2 mg/mL (or 4 mg/mL) was spin-coated on UV–O_3 treated ITO at 1000 r/min for 90 s to prepare a signal electron transport layer (ETL). A active layer solution of P3HT:$PC_{61}BM$ comprised of 20 mg/mL P3HT and 16 mg/mL $PC_{61}BM$ solution in 1 mL of ODCB was heated in 60°C and stirred sufficiently overnight, then deposited onto ITO/fullerene derivatives layer (formed by 2.0 and 4.0 mg/mL at 1000 r/min for 90 s) by spin-coating at 600 r/min for 100 s. After evaporation of the ODCB solvent in a vacuum for 1 h, the ternary blend films were thermally annealed at 150°C for 15 min inside a glovebox filled with N_2 prior to deposition of the cathodes. The fullerene derivatives C_{60}-2EPM layer (formed by 2.0 and 4.0 mg/mL at 1000 r/min for 60 s) was formed on ZnO to prepare bilayer ETLs at 1000 r/min for 90 s, then a solution containing a mixture of PTB7-Th:$PC_{71}BM$ (10 mg/mL:15 mg/mL) in a mixed solvent of dichlorobenzene/1,8-diiodooctane (97:3 v/v) was spin-cast on top of the bilayer ETL to produce a 100 nm thick active layer and the device was placed inverted in glove box for 1 h, followed by evaporation of the solvent in a vacuum.

2.4.2   Fabrication of ternary inverted OSCs

By introducing the additive of fullerene derivatives C_{60}-2EPM, the ternary photoactive layer blend of P3HT:$PC_{61}BM$:C_{60}-2EPM with the blending weight ratio of P3HT to the total acceptor materials ($PC_{61}BM$ plus C_{60}-2EPM) kept at 20 mg:16 mg (in wt%) in 1 mL o-dichlorobenzene was formed. The ternary photoactive layer blend was prepared relying on different weight ratios (0, 5, 10, 15, 20 wt%, respectively, relative to P3HT) of C_{60}-2EPM, then spin-coated on ZnO at 600 r/min for 100 s. After evaporation of the ODCB solvent in a vacuum for 1 h, the ternary blend films were then thermally annealed at 150°C for 15 min in an atmosphere of N_2.

Finally, a MoO_3 (6 nm) layer and then a top Al electrode (around 100 nm) were thermally deposited in a vacuum onto the photoactive layer at a pressure of 3.0×10^{-4} Pa. The active areas of the devices are all defined as 4 mm², which was defined by the overlapping area of the ITO and Al electrodes. The solar cells were characterized with a Keithley 2400 source meter under simulated AM 1.5 solar illumination at 100 mW/cm², calibrated with a silicon solar reference cell (SRC-1000-RTD).

2.5   X-ray photoelectron spectroscopy (XPS) measurements

The measurement of X-ray photoelectron spectroscopy (XPS) was carried out on ZnO and ZnO/C_{60}-2EPM layer to research the origin of the different morphology. The O 1s XPS spectrum of bare ZnO exhibits two typical peaks, located at about 529.8 and 531.0 eV (Fig. 2(a)). The peak at lower binding energy corresponds to the Zn-O bonds. The other peak at higher binding energy is ascribed to oxygen atoms from hydroxyl oxygen. Besides the two peaks from ZnO, the other peak (~531.8 eV) from C_{60}-2EPM appears for O 1s XPS spectrum of the ZnO modified by C_{60}-EPM, which associated with O-C-O. Due to the O-C-O chain, the new peaks for O 1s XPS spectrum of ZnO/C_{60}-2EPM is originated from ether chain. Figure 2(b) presents the C 1s XPS spectra of ZnO and ZnO/C_{60}-2EPM. It is found that all the samples have two peaks ~285 eV (O-C-O) and ~288.6 eV (COOR), which is assigned to the C atoms of carbonyl groups. The atomic concentrations of carbon, oxygen and zinc in all the samples based on the O 1s, C 1s and Zn 2p XPS spectra are summarized in Fig. 2(c). When C_{60}-2EPM were spin coated on the top of ZnO, the ether chain tend to the ZnO surface, leaving the hydrophobic and carbon-rich fullerene cage facing toward the opposite direction. In that case, more carbon and less zinc were detected. The XPS spectra of all atomics of ZnO and ZnO/C_{60}-2EPM were showed in Fig. S4. Compared with ZnO, the device of ZnO/C_{60}-2EPM appeared an obvious peak of C1s, which was root in C_{60}-2EPM.

2.6   Ultraviolet photo-electron spectroscopy (UPS) measurements

Ultraviolet photo-electron spectroscopy (UPS) was employed to clarify the energy level of the ZnO and ZnO/C_{60}-2EPM (showed in Fig. S5). The highest occupied
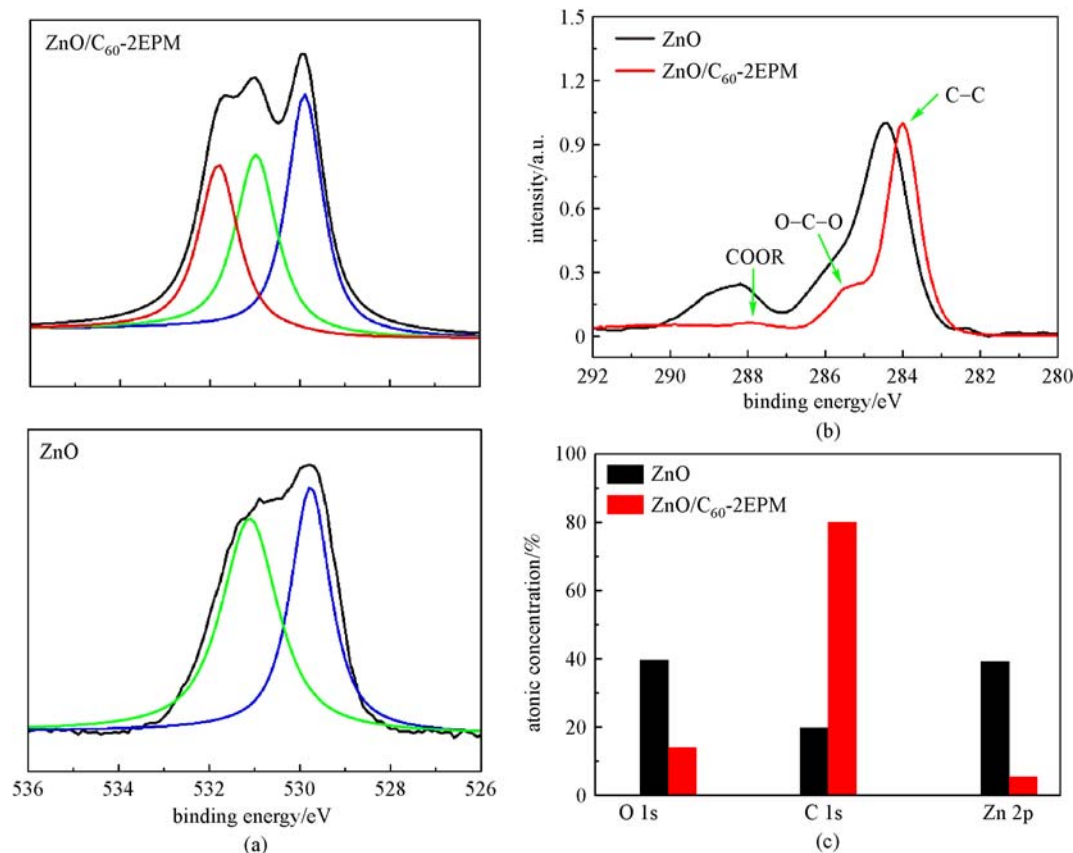
Fig. 2 (a) O 1s, (b) C 1s spectra of ZnO and ZnO/C$_{60}$-2EPM and (c) atomic concentrations of carbon, oxygen and zinc based on the corresponding XPS spectra

molecular orbital (HOMO) level energies are defined according to the Eq. (1) (where $h\nu$ was the incident photon energy of 21.2 eV, and E_{cutoff} was gained from the high binding energy cutoff of a spectrum, and E_{onset}^{HOMO} was delivered from the right panel).

$$E_{HOMO} = h\nu - (E_{onset}^{HOMO} - E_{cutoff}). \tag{1}$$

The HOMO energies for ZnO and ZnO/C$_{60}$-2EPM were −7.75 and −7.06 eV, respectively. According to the optical band gap obtained from the UV-vis absorption spectrum and HOMO energy levels, the LUMO energy levels were estimated to be −4.65 eV for ZnO and −4.08 eV for ZnO/C$_{60}$-2EPM, as summarized in Table 1. The band gap for ZnO and ZnO/C$_{60}$-2EPM were obtained from UV-vis absorption spectrum, which were 3.10 and 3.02 eV (as showed in Fig. S6(a)).

3 Result and discussion

To explore the function of the amphiphilic diblock fullerene derivatives as an ETL in OSCs, the single ETL inverted devices based on P3HT:PC$_{61}$BM were fabricated

Table 1 Energy levels of ZnO and ZnO/C$_{60}$-2EPM

Buffer layer	E_g	HOMO (UPS)	LUMO (E_g)
ZnO	3.10	−7.75	−4.65
ZnO/C$_{60}$-2EPM	3.02	−7.06	−4.04

with the structure of ITO/fullerene derivatives/P3HT: PC$_{61}$BM/MoO$_3$/Al. The illuminated current density–voltage (*J–V*) curves of the inverted device was shown in Fig. 3(a), and the corresponding device data was summarized in Table 2. The device without fullerene derivatives ETLs exhibits a very low photovoltaic performance with an open-circuit voltage (V_{oc}) of 0.39 V, short-circuit current density (J_{sc}) of 8.83 mA/cm^2, fill factor (*FF*) of 37.7% and PCE of only 1.30%. Fortunately, the device efficiencies were dramatically enhanced after insertion of the fullerene derivatives interface layer between ITO and the active layer, with a PCE of 2.12% for 2 mg/mL and 2.37% for 4 mg/mL. It should be noted that the device parameters, including V_{oc}, J_{sc}, and PCE, were improved simultaneously while keeping the *FF* had a little change. The dark current curves were shown in Fig. 3(c). This enhanced

Table 2 Device parameters of the inverted OSCs with the structure of ITO/ETL/active layer/MoO$_3$/Al with and without the fullerene derivatives as interface layers based on the blend system of P3HT:PC$_{61}$BM and PTB7-Th:PC$_{71}$BM under the illumination of AM 1.5 G, illumination at 100 mW/cm^2

ETL (mg·mL^{-1})	active layer	V_{oc}/V	J_{sc}/(mA·cm^{-2})	FF/%	PCE/%
ITO	P3HT:PC$_{61}$BM	0.39	8.83	37.70	1.30
ITO/C$_{60}$-2EPM (2.0)	P3HT:PC$_{61}$BM	0.49	11.92	36.14	2.12
ITO/C$_{60}$-2EPM (4.0)	P3HT:PC$_{61}$BM	0.49	12.32	39.16	2.37
ZnO	PTB7-Th:PC$_{71}$BM	0.78	16.72	62.36	8.11
ZnO/C$_{60}$-2EPM (2.0)	PTB7-Th:PC$_{71}$BM	0.78	16.79	63.82	8.38
ZnO/C$_{60}$-2EPM (4.0)	PTB7-Th:PC$_{71}$BM	0.78	16.94	65.14	8.65
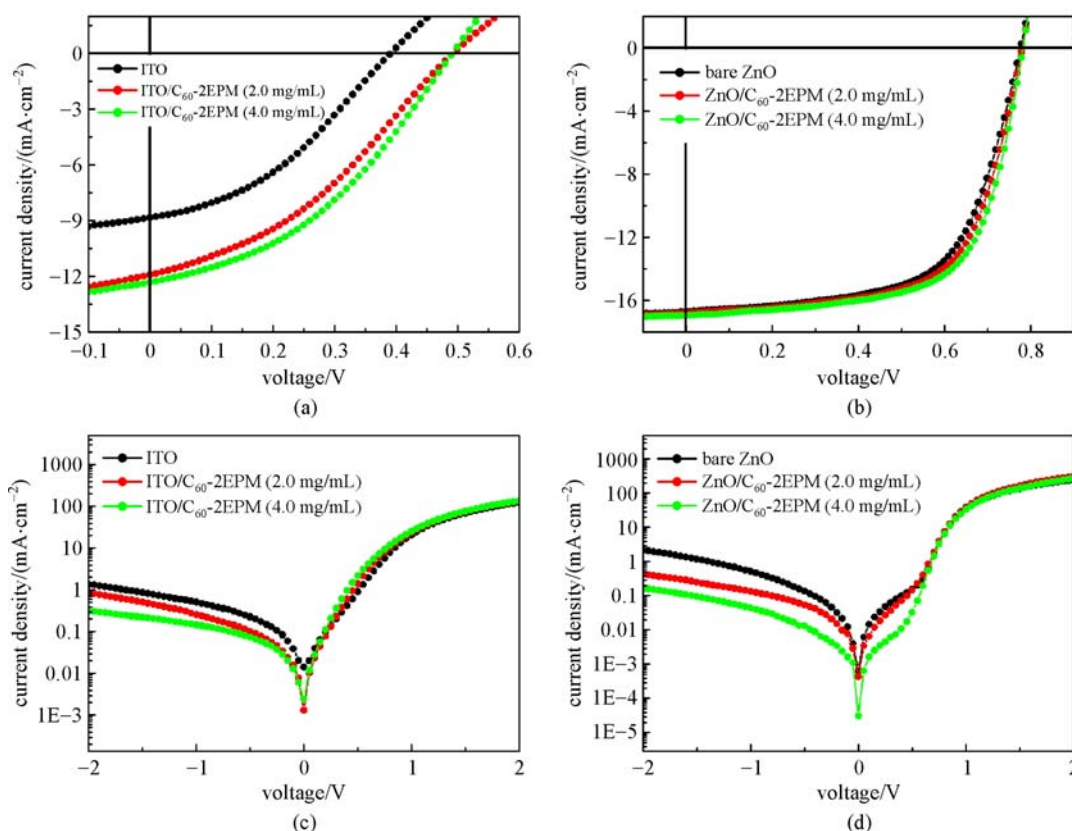
Fig. 3 *J–V* characteristics and dark current of the inverted polymer solar cell with different structure of (a)ITO/ fullerene derivatives (*x*)/ P3HT:PC$_{61}$BM/MoO$_3$/Al; (b) ITO/ZnO/fullerene derivatives (*x*)/PTB7-Th:PC$_{71}$BM /MoO$_3$/Al; (c) ITO/fullerene derivatives (*x*)/P3HT: PC$_{61}$BM/MoO$_3$/Al; (d) ITO/ZnO/fullerene derivatives (*x*)/PTB7-Th:PC$_{71}$BM/MoO$_3$/Al (*x* = 2.0, 4.0 mg/mL)

device performance was derived from the improved energy alignment in the device and optimized morphologies of both the fullerene derivatives interlayer and active layer. The author considered that the enhancement of PCE was caused by the better compatibility efficiency formed between the fullerene derivatives C$_{60}$-2EPM and ITO electrode.

To further verify and testify the universality of the amphiphilic diblock fullerene derivatives ETLs, inverted OSCs devices with bilayer ETLs were fabricated with

structure of ITO/ZnO/fullerene derivatives/PTB7-Th: PC$_{71}$BM/MoO$_3$/Al. The surface topography atomic force microscopy (AFM) images of the devices with structure of ITO/ZnO/C$_{60}$-2EPM (*x* = 0, 2.0 and 4.0 mg/mL) were showed in Fig. S7, which indicated that the fullerene derivatives layer formed in fold sharp with the increasing concentrations of C$_{60}$-2EPM coated on ZnO. The photovoltaic performance curves based on PTB7-Th:PC$_{71}$BM blend was displayed in Fig. 3(b) and the corresponding data were summarized in Table 2. Analogous to the

average PCE of ZnO (8.11%), the average efficiencies of the ZnO/C$_{60}$-2EPM modified devices was as high as 8.38% for 2 mg/mL and 8.65% for 4 mg/mL, respectively. The notable efficiencies based on the ZnO/C$_{60}$-2EPM bilayer interface layer should be ascribed to the simultaneous enhancement of *FF*. The *FF* was enhanced from 62.36% to 63.82% and 65.14% for devices based on two different connections, respectively. The dark current curves were shown in Fig. 3(d), in which it is obvious that the dark current densities of the ZnO/C$_{60}$-2EPM interfacial layers under reverse bias are smaller than that of the bare ZnO interfacial layer.

For convenience, *x*% abbreviation was used to be a device abbreviation for a ternary blend system with different weight ratio of C$_{60}$-2EPM relative to PC$_{61}$BM. For example, the 5% device was supported a ternary blend system including a ratio of P3HT:PC$_{61}$BM:C$_{60}$-2EPM (1:0.76:0.04 in wt%). A series of different proportions (0%, 5%, 10%, 15% and 20%) of ternary blend devices were fabricated to study the effect of C$_{60}$-2EPM between donor and acceptor. As showed in Fig. S8, by introducing C$_{60}$-2EPM in ternary blend, the devices have got better surface topography AFM images of P3HT:PC$_{61}$BM:C$_{60}$-2EPM (*x*%) layer than device without addition. The absorption of the device with the structure of ITO/ZnO/P3HT:PC$_{61}$BM:C$_{60}$-2EPM (*x*%) were showed in Fig. S6 (b), it indicated that the addition of fullerene derivatives

have a negligible effect on the absorption of devices. The devices with ternary blend of P3HT:PC$_{61}$BM:C$_{60}$-2EPM (*x* %) all showed better performance than 0% devices (Table 3). The photovoltaic performance curves of ternary device based on P3HT:PC$_{61}$BM were displayed in Fig. 4(a). For the ternary blend, it showed that devices with weight ratios of 5%, 10%, 15% and 20% have got PCEs of 3.64%, 3.84%, 3.87% and 3.76%, comparing with 3.94% of the 0% device. This result implied that the introduction of C$_{60}$-2EPM (5%–20%) in the active layer could cause an obvious influence on the PCEs of the P3HT:PC$_{61}$BM system. The author considered that C$_{60}$-2EPM could induce P3HT to arrange in an ordered manner with annealing via the direct molecular interaction between the ether chain groups of C$_{60}$-2EPM and the hexyl groups of P3HT. An excess amount of fullerene derivatives additive could also lead a contrary effect on the PCE of OSCs by affecting the proportion and interaction between P3HT and PC$_{61}$BM. The dark current densities of the device with addition of C$_{60}$-2EPM (5%, 10%, 15% and 20%) under reverse bias are smaller than that of device without addition (showed in Fig. 4(b)), which means that the leakage current at negative voltages was greatly inhibited by the addition of C$_{60}$-2EPM. The dark current curve also demonstrates that the addition of C$_{60}$-2EPM could reduce the leakage current and enhances the charge injection efficiency.

Table 3 Photovoltaic parameters of the ternary inverted OSCs with the structure of ITO/ZnO/P3HT:PC$_{61}$BM:C$_{60}$-2EPM(*x*)/MoO$_3$/Al

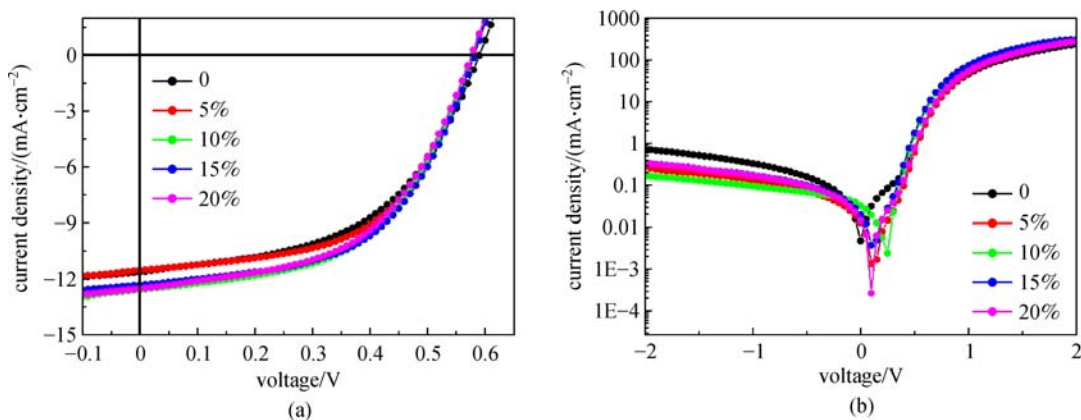| additive	ratio/wt%	V_{oc}/V	J_{sc}/(mA·cm^{-2})	*FF*/%	PCE/%
	0	0.59	11.62	50.91	3.49
C$_{60}$-2EPM	5	0.58	11.53	54.35	3.64
C$_{60}$-2EPM	10	0.58	12.57	52.84	3.84
C$_{60}$-2EPM	15	0.58	12.32	54.15	3.87
C$_{60}$-2EPM	20	0.58	12.52	52.06	3.76

Fig. 4 (a) *J*–*V* characteristics; (b) dark current of the inverted polymer solar cell with structure of ITO/ZnO/P3HT:PC$_{61}$BM:C$_{60}$-2EPM (*x* = 0, 5%, 10%, 15% and 20%)

4   Conclusions

The synthesized ether chain functionalized fullerene derivatives C_{60}-2EPM was reported as ETL in PTB7-Th:C_{71}BM and additive in P3HT:PC_{61}BM in inverted OSCs. When applied as ETLs, the fullerene derivatives could self-assemble onto the ZnO surface due to the ether chain and modified the ZnO surface defects. Compared with the control devices without fullerene derivatives, the obtained ZnO/C_{60}-2EPM modified devices realize efficient electron transfer from active layer to electrode, which can be attributed to the PCBM of fullerene derivatives. When selecting thermal-annealing-free PTB7-Th:C_{71}BM as the photoactive layer, device efficiencies of 8.38% and 8.65% for 2.0 and 4.0 mg/mL were obtained respectively after introduction of C_{60}-2EPM. When used as an additive in the active layer of P3HT:PC_{61}BM, all the devices with addition from 5%, 10%, 15% to 20% exhibited got better PCEs than device without additive. The 15% device of C_{60}-2EPM showed the best PCE of 3.87%. The results are particularly interesting to develop buffer layer materials in inverted OSCs toward high efficiency and longer lifetime.

Acknowledgements

Supporting Information

Additional figures as mentioned in the text, include ^{1}H NMR spectrum, UV-vis absorption spectrum, XPS spectra, UPS spectra and surface topography AFM images.
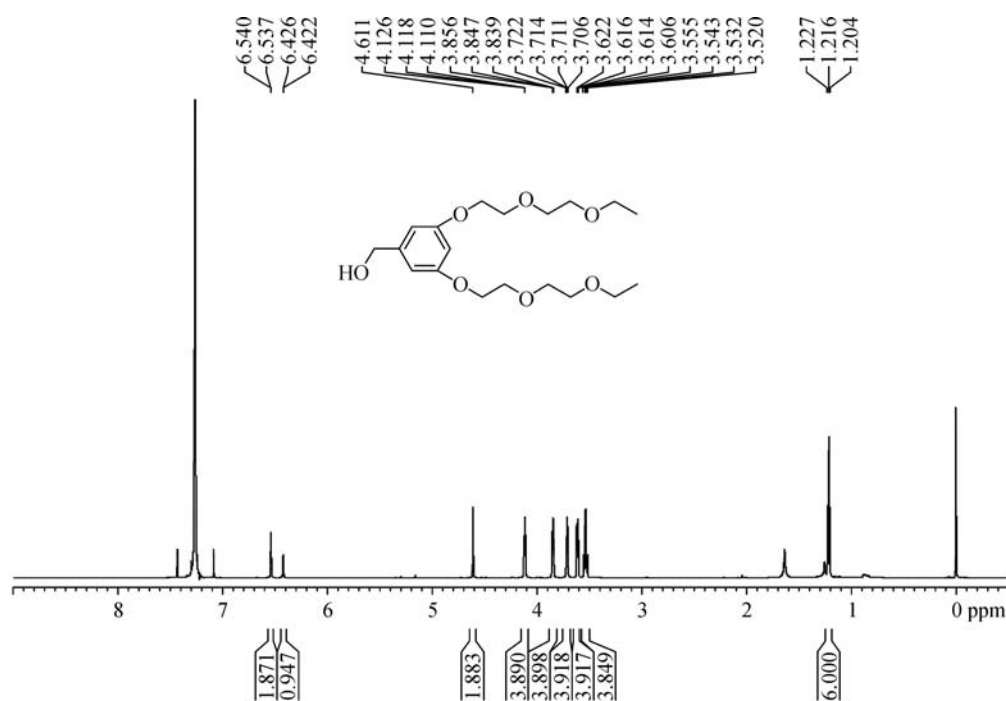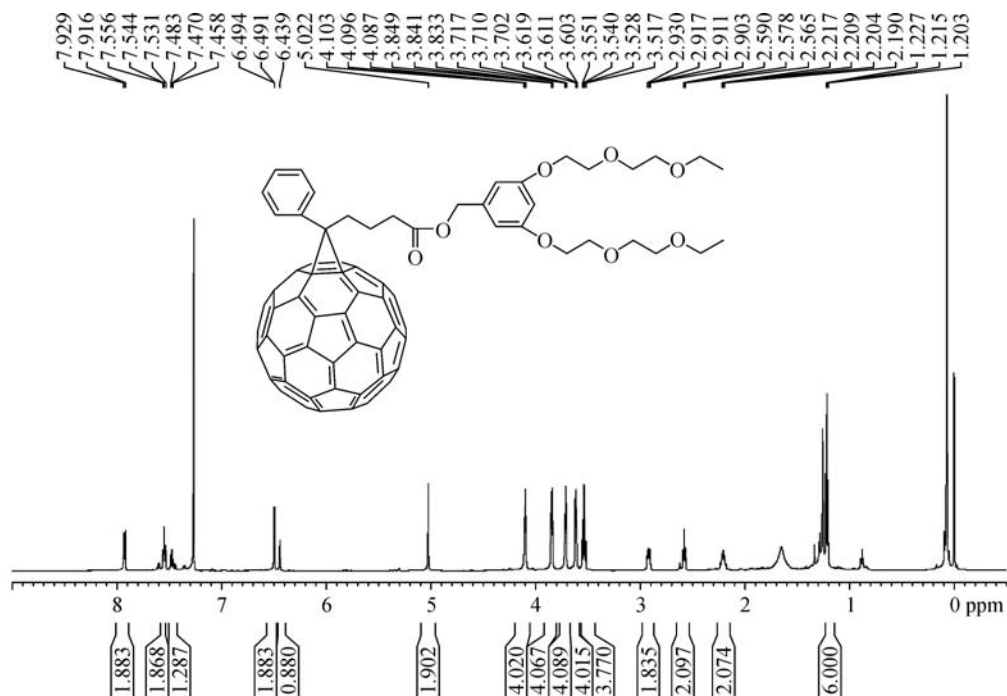

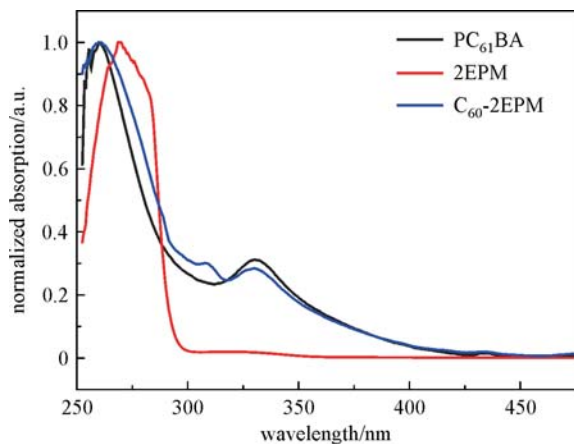**Fig. S1** ^{1}H NMR spectrums of 2EPM

Fig. S2 ^{1}H NMR spectrums of C_{60}-2EPM

Fig. S3 UV-vis absorption spectrum of the $PC_{61}BA$, 2EPM and C_{60}-2EPM
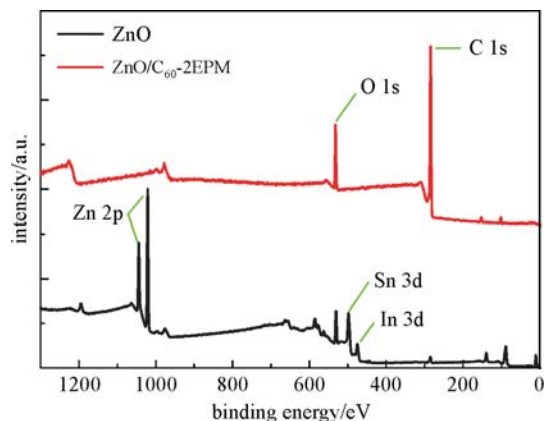
Fig. S4 XPS spectra of all atomics of ZnO and ZnO/C_{60}-2EPM
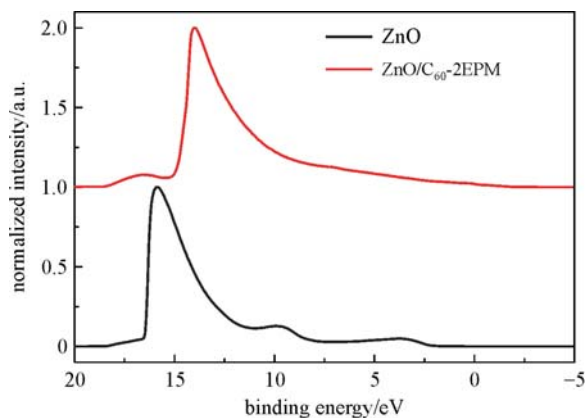

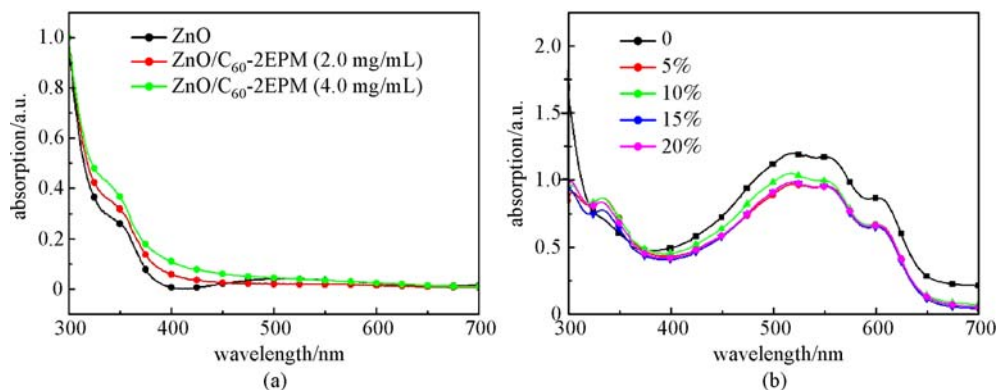**Fig. S5** UPS spectra of ZnO and ZnO/C_{60}-2EPM

Fig. S6   UV-vis absorption spectrum of (a) ZnO and ZnO/C_{60}-2EPM; (b) the devices with the structure of ITO/ZnO/P3HT:PC$_{61}$BM:C_{60}-2EPM (x = 0, 5%, 10%, 15% and 20%)
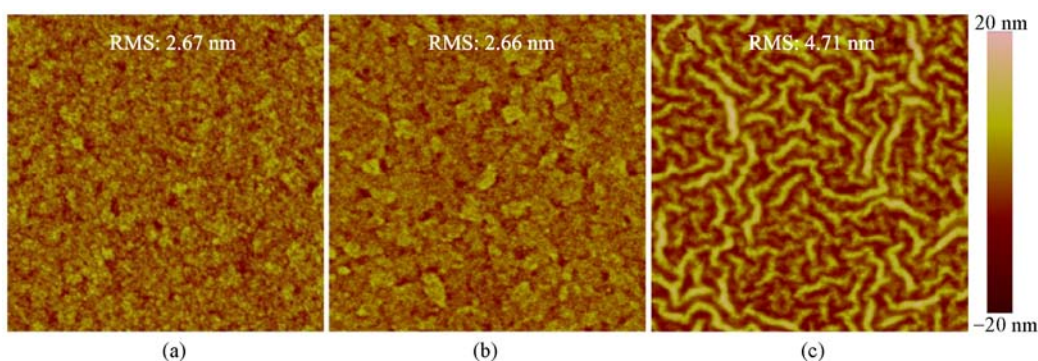

Fig. S7   Surface topography AFM images (5 μm × 5 μm) of the devices. (a) ITO/ZnO/; (b) ITO/ZnO/C_{60}-2EPM (2.0 mg/mL); (c) ITO/ZnO/C_{60}-2EPM (4.0 mg/mL)
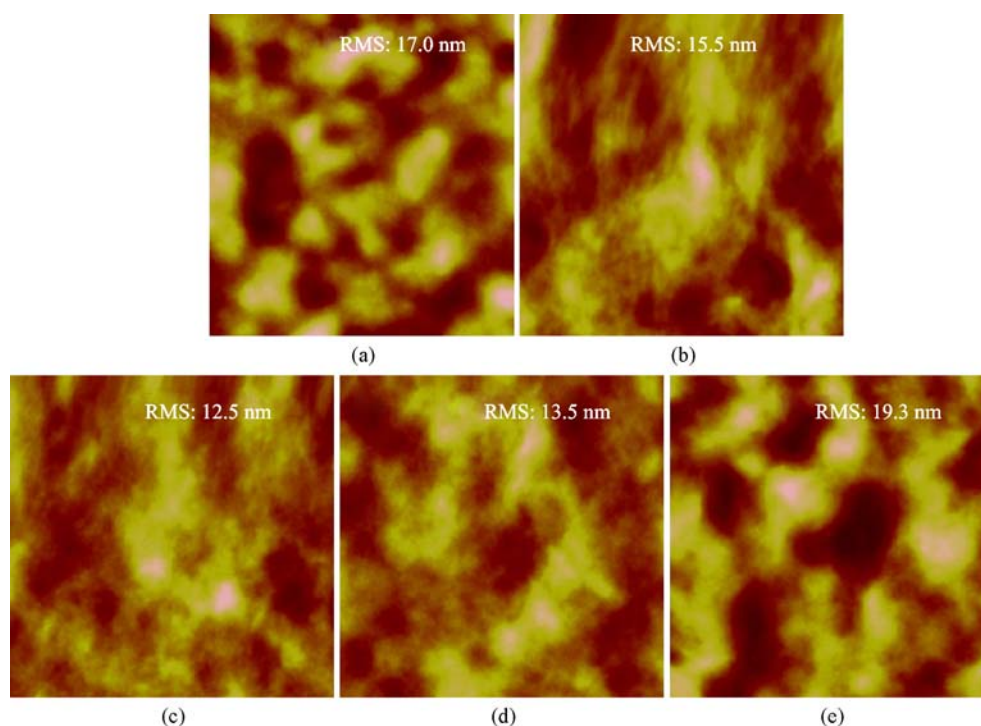

Fig. S8   Surface topography AFM images (5 μm × 5 μm) of devices with the structure of ITO/ZnO/P3HT:PC$_{61}$BM with addition of C_{60}-2EPM. (a) 0%; (b) 5% C_{60}-2EPM; (c) 10% C_{60}-2EPM; (d) 15% C_{60}-2EPM; (e) 20% C_{60}-2EPM

Notes

The authors declare no competing financial interest.

References

1. Deng W, Gao K, Yan J, Liang Q, Xie Y, He Z, Wu H, Peng X, Cao Y. Origin of reduced open-circuit voltage in highly efficient small-molecule-based solar cells upon solvent vapor annealing. ACS Applied Materials & Interfaces, 2018, 10(9): 8141–8147

2. Liao S H, Jhuo H J, Cheng Y S, Gupta V, Chen S A. A high performance inverted organic solar cell with a low band gap small molecule (*p*-DTS(FBTTh₂)₂) using a fullerene derivative-doped zinc oxide nano-film modified with a fullerene-based self-assembled monolayer as the cathode. Journal of Materials Chemistry A, Materials for Energy and Sustainability, 2015, 3(45): 22599–22604

3. Papamakarios V, Polydorou E, Soultati A, Droseros N, Tsikritzis D, Douvas A M, Palilis L, Fakis M, Kennou S, Argitis P, Vasilopoulou M. Surface modification of ZnO layers via hydrogen plasma treatment for efficient inverted polymer solar cells. ACS Applied Materials & Interfaces, 2016, 8(2): 1194–1205

4. Singh S P, Kumar C H P, Nagarjuna P, Kandhadi J, Giribabu L, Chandrasekharam M, Biswas S, Sharma G D. Efficient solution processable polymer solar cells using newly designed and synthesized fullerene derivatives. Journal of Physical Chemistry C, 2016, 120(35): 19493–19503

5. Wu Y, Zou Y, Yang H, Li Y, Li H, Cui C, Li Y. Achieving over 9.8% efficiency in nonfullerene polymer solar cells by environmentally friendly solvent processing. ACS Applied Materials & Interfaces, 2017, 9(42): 37078–37086

6. Zhao F, Dai S, Wu Y, Zhang Q, Wang J, Jiang L, Ling Q, Wei Z, Ma W, You W, Wang C, Zhan X. Single-junction binary-blend nonfullerene polymer solar cells with 12.1% efficiency. Advanced Materials, 2017, 29(18): 1700144

7. Zhao W, Li S, Yao H, Zhang S, Zhang Y, Yang B, Hou J. Molecular optimization enables over 13% efficiency in organic solar cells. Journal of the American Chemical Society, 2017, 139(21): 7148–7151

8. Chakravarthi N, Gunasekar K, Cho W, Long D X, Kim Y H, Song C E, Lee J C, Facchetti A, Song M, Noh Y Y, Jin S H. A simple structured and efficient triazine-based molecule as an interfacial layer for high performance organic electronics. Energy & Environmental Science, 2016, 9(8): 2595–2602

9. George Z, Xia Y, Sharma A, Lindqvist C, Andersson G, Inganäs O, Moons E, Müller C, Andersson M R. Two-in-one: cathode modification and improved solar cell blend stability through addition of modified fullerenes. Journal of Materials Chemistry A, Materials for Energy and Sustainability, 2016, 4(7): 2663–2669

10. Jeong M, Chen S, Lee S M, Wang Z, Yang Y, Zhang Z G, Zhang C, Xiao M, Li Y, Yang C. Feasible D1-A-D2-A random copolymers for simultaneous high-performance fullerene and nonfullerene solar cells. Advanced Energy Materials, 2018, 8(7): 1702166

11. Kim T, Younts R, Lee W, Lee S, Gundogdu K, Kim B J. Impact of the photo-induced degradation of electron acceptors on the photophysics, charge transport and device performance of all-polymer and fullerene–polymer solar cells. Journal of Materials Chemistry A, Materials for Energy and Sustainability, 2017, 5(42): 22170–22179

12. Wang W, Song L, Magerl D, Moseguí González D, Körstgens V, Philipp M, Moulin J F, Müller-Buschbaum P. Influence of solvent additive 1,8-octanedithiol on P3HT:PCBM solar cells. Advanced Functional Materials, 2018, 28(20): 1800209

13. Cai X, Yuan T, Liu X, Tu G. Self-assembly of 1-pyrenemethanol on ZnO surface toward combined cathode buffer layers for inverted polymer solar cells. ACS Applied Materials & Interfaces, 2017, 9(41): 36082–36089

14. Lu S, Lin H, Zhang S, Hou J, Choy W C H. A switchable interconnecting layer for high performance tandem organic solar cell. Advanced Energy Materials, 2017, 7(21): 1701164

15. Zhang F, Shi W, Luo J, Pellet N, Yi C, Li X, Zhao X, Dennis T J S, Li X, Wang S, Xiao Y, Zakeeruddin S M, Bi D, Grätzel M. Isomer-pure bis-PCBM-assisted crystal engineering of perovskite solar cells showing excellent efficiency and stability. Advanced Materials, 2017, 29(17): 1606806

16. Choi H, Mai C K, Kim H B, Jeong J, Song S, Bazan G C, Kim J Y, Heeger A J. Conjugated polyelectrolyte hole transport layer for inverted-type perovskite solar cells. Nature Communications, 2015, 6(1): 7348

17. Lange I, Reiter S, Pätzel M, Zykov A, Nefedov A, Hildebrandt J, Hecht S, Kowarik S, Wöll C, Heimel G, Neher D. Tuning the work function of polar zinc oxide surfaces using modified phosphonic acid self-assembled monolayers. Advanced Functional Materials, 2014, 24(44): 7014–7024

18. Nam S, Seo J, Song M, Kim H, Ree M, Gal Y S, Bradley D D C, Kim Y. Polyacetylene-based polyelectrolyte as a universal interfacial layer for efficient inverted polymer solar cells. Organic Electronics, 2017, 48: 61–67

19. Cheng Y J, Cao F Y, Lin W C, Chen C H, Hsieh C H. Self-assembled and cross-linked fullerene interlayer on titanium oxide for highly efficient inverted polymer solar cells. Chemistry of Materials, 2011, 23(6): 1512–1518

20. Seo J H, Gutacker A, Sun Y, Wu H, Huang F, Cao Y, Scherf U, Heeger A J, Bazan G C. Improved high-efficiency organic solar cells via incorporation of a conjugated polyelectrolyte interlayer. Journal of the American Chemical Society, 2011, 133(22): 8416–8419

21. Zhou D, Xiong S, Chen L, Cheng X, Xu H, Zhou Y, Liu F, Chen Y. A green route to a novel hyperbranched electrolyte interlayer for nonfullerene polymer solar cells with over 11% efficiency. Chemical Communications (Cambridge), 2018, 54(5): 563–566

22. Chao Y H, Huang Y Y, Chang J Y, Peng S H, Tu W Y, Cheng Y J, Hou J, Hsu C S. A crosslinked fullerene matrix doped with an ionic fullerene as a cathodic buffer layer toward high-performance and thermally stable polymer and organic metallohalide perovskite solar cells. Journal of Materials Chemistry A, Materials for Energy and Sustainability, 2015, 3(40): 20382–20388

23. Zhang J, Xue R, Xu G, Chen W, Bian G Q, Wei C, Li Y, Li Y. Self-doping fullerene electrolyte-based electron transport layer for all-room-temperature-processed high-performance flexible polymer solar cells. Advanced Functional Materials, 2018, 28(13): 1705847

24. Zhao F, Wang Z, Zhang J, Zhu X, Zhang Y, Fang J, Deng D, Wei Z, Li Y, Jiang L, Wang C. Self-doped and crown-ether functionalized

fullerene as cathode buffer layer for highly-efficient inverted polymer solar cells. Advanced Energy Materials, 2016, 6(9): 1502120

25. Cui C, Li Y, Li Y. Fullerene derivatives for the applications as acceptor and cathode buffer layer materials for organic and perovskite solar cells. Advanced Energy Materials, 2017, 7(10): 1601251

26. Derue L, Dautel O, Tournebize A, Drees M, Pan H, Berthumeyrie S, Pavageau B, Cloutet E, Chambon S, Hirsch L, Rivaton A, Hudhomme P, Facchetti A, Wantz G. Thermal stabilisation of polymer-fullerene bulk heterojunction morphology for efficient photovoltaic solar cells. Advanced Materials, 2014, 26(33): 5831–5838

27. Duan C, Zhang K, Zhong C, Huang F, Cao Y. Recent advances in water/alcohol-soluble π-conjugated materials: new materials and growing applications in solar cells. Chemical Society Reviews, 2013, 42(23): 9071–9104

28. Liu J, Ji Y, Liu Y, Xia Z, Han Y, Li Y, Sun B. Doping-free asymmetrical silicon heterocontact achieved by integrating conjugated molecules for high efficient solar cell. Advanced Energy Materials, 2017, 7(19): 1700311

29. Pal A, Wen L K, Jun C Y, Jeon I, Matsuo Y, Manzhos S. Comparative density functional theory-density functional tight binding study of fullerene derivatives: effects due to fullerene size, addends, and crystallinity on band structure, charge transport and optical properties. Physical Chemistry Chemical Physics, 2017, 19(41): 28330–28343

30. Zhang Z G, Li H, Qi B, Chi D, Jin Z, Qi Z, Hou J, Li Y, Wang J. Amine group functionalized fullerene derivatives as cathode buffer layers for high performance polymer solar cells. Journal of Materials Chemistry A, Materials for Energy and Sustainability, 2013, 1(34): 9624

31. Zhang F L, Gadisa A, Inganäs O, Svensson M, Andersson M R. Influence of buffer layers on the performance of polymer solar cells. Applied Physics Letters, 2004, 84(19): 3906–3908

32. Li Y, Zhao Y, Chen Q, Yang Y M, Liu Y, Hong Z, Liu Z, Hsieh Y T, Meng L, Li Y, Yang Y. Multifunctional fullerene derivative for interface engineering in perovskite solar cells. Journal of the American Chemical Society, 2015, 137(49): 15540–15547

33. Liu J, Li J, Liu X, Li F, Tu G. Amphiphilic diblock fullerene derivatives as cathode interfacial layers for organic solar cells. ACS Applied Materials & Interfaces, 2018, 10(3): 2649–2657

34. Nguyen T L, Lee T H, Gautam B, Park S Y, Gundogdu K, Kim J Y, Woo H Y. Single component organic solar cells based on oligothiophene-fullerene conjugate. Advanced Functional Materials, 2017, 27(39): 1702474

35. Chen Y, Qin Y, Wu Y, Li C, Yao H, Liang N, Wang X, Li W, Ma W, Hou J. From binary to ternary: improving the external quantum efficiency of small-molecule acceptor-based polymer solar cells with a minute amount of fullerene sensitization. Advanced Energy Materials, 2017, 7(17): 1700328

36. Hodgkiss J M, Tu G, Albert-Seifried S, Huck W T S, Friend R H. Ion-induced formation of charge-transfer states in conjugated polyelectrolytes. Journal of the American Chemical Society, 2009, 131(25): 8913–8921

37. Hummelen J C, Knight B W, Lepeq F, Wudl F, Yao J, Wilkins C L. Preparation and characterization of fulleroid and methanofullerene derivatives. Journal of Organic Chemistry, 1995, 60(3): 532–538

38. Lee H K H, Telford A M, Röhr J A, Wyatt M F, Rice B, Wu J, de Castro Maciel A, Tuladhar S M, Speller E, McGettrick J, Searle J R, Pont S, Watson T, Kirchartz T, Durrant J R, Tsoi W C, Nelson J, Li Z. The role of fullerenes in the environmental stability of polymer: fullerene solar cells. Energy & Environmental Science, 2018, 11(2): 417–428

39. Yamada M, Ochi R, Yamamoto Y, Okada S, Maeda Y. Transition-metal-catalyzed divergent functionalization of [60]fullerene with propargylic esters. Organic & Biomolecular Chemistry, 2017, 15(40): 8499–8503

Jikang Liu received his B.S. degree in 2014 from the Huazhong University of Science and Technology, China. In 2014, he joined the energy photoelectron functional laboratory of Wuhan National Laboratory for Optoelectronics and studied in the organic solar cells group. His main research interests include the preparation of organic solar cells devices and the self-assembly of fullerene derivatives.

Junli Li received her B.S. degree in 2014 from the Luoyang Normal University, China. In 2014, she joined the energy photoelectron functional laboratory of Wuhan National Laboratory for Optoelectronics and studied in the organic solar cells group. Her main research interests include the preparation of organic solar cells and organic light emitting diode devices.

Guoli Tu received his B.S. degree in 1996 from the Jilin University, China. He received his Ph.D. degree from Changchun Institute of Applied Chemistry, Chinese Academy of Sciences, in 2003. From 2004 to 2006, he was engaged in postdoctoral research in Wuppertal University, Germany. From 2006 to 2009, he was engaged in postdoctoral research in the department of University of Cambridge, UK. From 2009, he is appointed as a professor of Wuhan National Laboratory for Optoelectronics at Huazhong University of Science and Technology. His main research interests include organic solar cells materials and devices, organic light emitting diode materials and devices, and polyimide materials and films.